

Improving Optics Control and Measurement at RHIC

William Fung^a, Yue Hao^a, Xiaofeng Gu^b, Robert-Demolaize Guillaume^b

^a*Department of Physics and Astronomy, Michigan State University, East Lansing, MI 48824, USA*

^b*Brookhaven National Laboratory, Upton, NY 11973, USA*

Abstract

In order to aid in luminosity maximization at the interaction point (IP), the collision location s_{IP} must be equivalent to the location of the minimum value of the beta function s^* . Accurate optics measurements and s^* movements are therefore essential to luminosity optimization. However, according to current Relativistic Heavy Ion Collider (RHIC) operations measurements, average horizontal beta beat measurements between operating IPs are around 20% along with significant variation in s^* measurements. A sensitivity matrix was shown to successfully move s^* and the linear optics to their desired values using power supply currents at the 8 o'clock interaction region (IR8). A method to measure the linear optics using the one-turn map within IRs was explored and compared with other mature methods. An error analysis was also included for all optics measurements methods. Through these methods, a 10% beat reduction was consistently achieved while moving s_x^* as well significant improvement to variations in s^* measurements. These methods used at the RHIC control room will be updated for future linear optics analysis and control.

Keywords: RHIC, Optics Correction, Interaction Region, Total Least Squares Regression

1. Introduction

The luminosity is vital in delivering high quality physics experiments at STAR and sPHENIX, located at IR6 and IR8 of the RHIC ring, respectively. The optics near each IR must be accurately controlled so that both colliding beams reach their desired beam sizes at the designed longitudinal position with respect to the detector location. We characterized the IR optics by the minimum of the beta function (β^*) located at s^* at each IR [21]. Therefore, precise measurements and adjustment of optics, especially of transverse s^* , is crucial to ensure maximal luminosity output.

In order to locally adjust or correct the optics within an collider ring without perturbing the global optics, a model-based tuning scheme utilizing the Jacobian solver in MAD-X (commonly referred to as MAD-X matching) is often employed [4, 13]. This technique has been extensively used at RHIC, for example, to match the derivative of the dispersion function at the Siberian snakes in order to preserve spin polarization [12]. However, due to the inherently nonlinear nature of the solver, the resulting magnet strengths can exhibit significant variation between successive iterations. Such fluctuations pose challenges for online optimization, where large, iterative changes in magnet settings are particularly susceptible to magnet hysteresis effects. As an alternative, this paper considers the use of an optics response matrix, or sensitivity matrix \mathbf{B} , which enables a linearized approach to optics correction with improved control over changes in magnet strengths [15].

Techniques to measure the beta function and minimize discrepancies between measured and model ones (beta-beat) using beam position monitors (BPMs) have evolved throughout the history of synchrotron research as documented in [18]. Beta from amplitude methods such as Harmonic Analysis [2] and

Model Independent Methods (MIA) [19] offer rapid and convenient means for optics measurements. However, these approaches are susceptible to systematic errors originating from BPM calibration and noise. Beta from phase advance such as 3-BPM [2] and N-BPM methods [10] demonstrate improved robustness towards BPM errors and eliminate calibration errors. While the N-BPM is more computationally intensive, various advancements have been developed to improve its computational efficiency [20].

Six initial TBT measurements from the proton-proton lattice without quadrupole modifications were taken to test the robustness of the current optics program at the RHIC control room. The mean and sample standard deviations of the beta measurements were taken as beta beat and error bars respectively as shown in Fig. 1. The average transverse beta beat was calculated to be within 20%. The error bars show more variation in measurements compared to past RHIC analysis [16].

The error from these measurements were then propagated from beta function to β^* and s^* at IP8 using a Monte Carlo method with 500 iterations, shown in Fig. 2. This analysis reveals a β^* beat variation of around 8% and 5% and s^* variation of around 27 and 18 cm at IP8 in the horizontal and vertical plane respectively. These BPM errors show high variance in measurement when multiple TBT measurements are made, leading to inconsistent measurements of the optics.

Since the sPHENIX detector has a vertex detection within ± 10 cm [1], more accurate and consistent s^* measurements and adjustments will greatly aid luminosity maximization.

All optics measurement methods mentioned until now depend on calculations from a lattice model such as MAD-X to determine the beta function. However, this dependency on the model could bias results towards model values, unintentionally

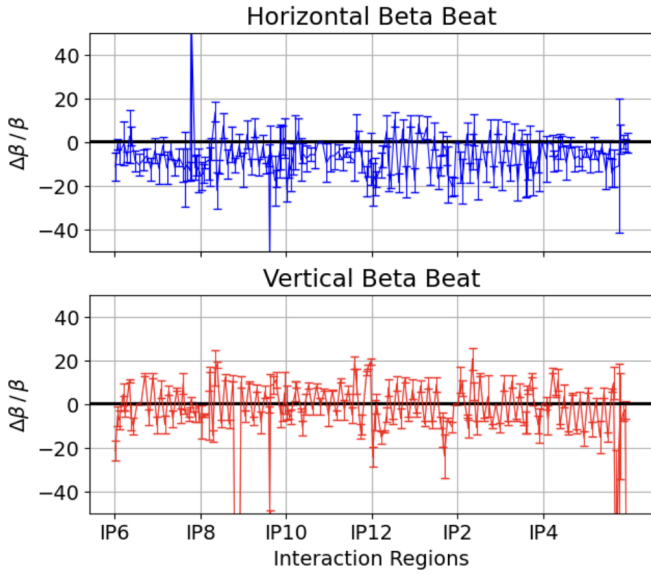


Figure 1: Measured horizontal (blue) and vertical (red) beta beat from curve fit method vs BPM number. The solid black lines indicate beta beat ± 2 . Error bars were calculated to be around 5% and 3% for horizontal and vertical axis respectively.

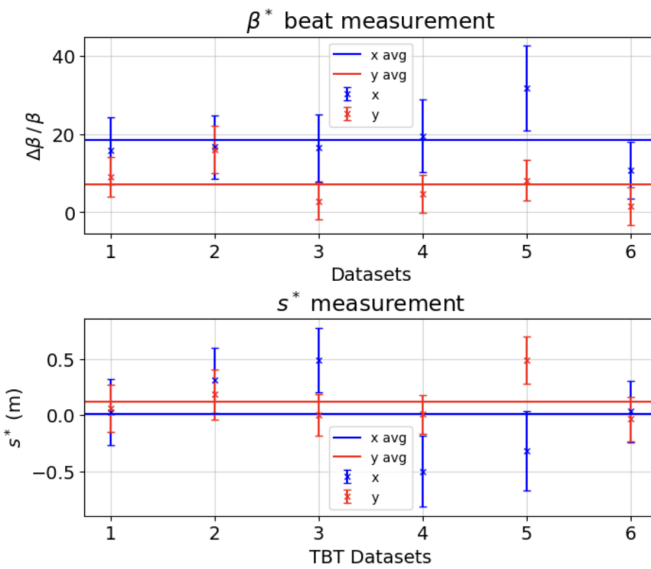


Figure 2: Measured horizontal (blue) and vertical (red) beta beat and s^* measurements at IP8 vs BPM number on the left and right respectively. Six TBT datasets with no movement of s^* ($\Delta s^* = 0$) were analyzed. Error bars were determined using 500 Monte Carlo iterations propagated from beta error values in Fig. 1.

skewing the results to match the model's beta function. Alternatively, a model independent method to measure the optics using the one-turn map at the IRs will be discussed and compared to various model-dependent methods, including measurements from the RHIC optics program. Previous studies measure the linear optics at RHIC using the one-turn map to measure global coupling [7]. However, since the optics are measured within sections with magnets, a lattice model was used.

This paper is structured in accordance with the following experimental procedure for the adjustments and measurement of β^* and s^* at the IRs. First, we introduce the proposed algorithm for adjusting s^* in Section 2. The calculation of the required currents changes is performed via a sensitivity matrix. These values are converted to magnet strengths and sent to RHIC control room. TBT measurements are taken after exciting the betatron motion by a fast kicker during RHIC operations. The resulting TBT data is preprocessed and then analyzed using various optics measurement methods described in Section 3 to calculate measured values of β^* and s^* . Finally, results and comparisons between different optics measurement methods are discussed in Section 4.

2. Optics tuning

To achieve better control of the optics at IR, an approach using the sensitivity matrix \mathbf{B} [15] was utilized, where \mathbf{B} represents an approximately linear relationship between the change in magnet strengths ΔK and change in optics ΔO . However, it is possible for the sensitivity matrix to request certain combinations of magnet strengths that may not be physically realizable in the actual machine due to hardware constraints in the power supply (PS) configuration [3]. For instance, in the interaction regions IR6 and IR8, quadrupoles 4-6 on both sides of the IR are powered by a single current supply, resulting in a total of six quadrupoles being controlled by one power source. Consequently, the optimization variables and constraints were defined in terms of PS currents \mathbf{I} rather than the magnet strengths. \mathbf{B} is therefore defined in this paper as the relation between $\Delta \mathbf{I}$ and $\Delta \mathbf{O}$:

$$\Delta \mathbf{O} = \mathbf{B} \Delta \mathbf{I} \quad (1)$$

\mathbf{I} consists of seventeen PS currents that affect an equal amount of insertion quadrupoles within IR8. \mathbf{O} includes thirteen optics parameters: transverse s^* , β^* , and horizontal dispersion at IP; and optics at the upstream end of IR8 (between insertion and arc regions): transverse β , α , μ , horizontal dispersion, and change in horizontal dispersion. The optics in \mathbf{O} were chosen to match preferred values of optics at IP and close the optics at the ends of IR8.

To calculate \mathbf{B} , the optics were first obtained to get \mathbf{O} , corresponding to the initial PS values \mathbf{I} . \mathbf{I} was then varied using a uniform distribution between $-1A$ and $1A$. This was to control PS values close to PS limits from exceeding such constraints. The resulting PS values $\Delta \mathbf{I}$ were then fed into the MAD-X RHIC lattice and the resulting $\Delta \mathbf{O}$ was obtained, where $\Delta \mathbf{O}$ is the change in the optics from the bare lattice values. A linear

regression was then performed to compute \mathbf{B} . A correlation coefficient close to one was measured, demonstrating linearity within $\pm 1A$.

As we will demonstrate in the experiment, to move s_x^* while keeping the other optical quantities constant, the currents required can be calculated from the pseudo-inverse of \mathbf{B} from Eq. (2). This can be extended to moving s_y^* or any other optical quantities in IR while maintaining certain constraints.

$$\Delta \mathbf{I}_0 = \mathbf{B}^{-1} \begin{bmatrix} \Delta s_x^* \\ 0 \\ \dots \\ 0 \end{bmatrix} \quad (2)$$

Altering magnet strengths would result in hysteresis effects if the change in magnet strengths were to change directions for the next movement s^* . To avoid hysteresis effects, a monotonicity constraint was imposed on the movement of magnet strengths, ensuring a consistent direction of values throughout the adjustment process. After each step in s^* , the allowable bounds on the magnet strengths were updated to respect this constraint. Additionally, to ensure safe operating conditions, a constraint was applied to the PS currents, requiring them to remain within $\pm 5A$ from their specified limits ($[\mathbf{I}_{min} + 5A, \mathbf{I}_{max} - 5A]$). When moving s^* , the adjustments to individual currents were also minimized in the penalty function to remain within a linear response regime and prevent abrupt transitions. We observed that the maximum ΔI_j during each movement did not exceed $5A$ after the optimization was done. These constraints are defined in Table 1. Respecting these constraints was made possible using the null space of \mathbf{B} using (3), as Eq. (1) is an under-determined system.

$$\Delta \mathbf{I}_C = \mathbf{B}^{-1} \begin{bmatrix} s_x^* \\ 0 \\ \dots \\ 0 \end{bmatrix} - \text{Null}(\mathbf{B})C \quad (3)$$

Where \mathbf{C} is a vector of constants whose size is the number of free parameters in the system (in this case, four). These are chosen such constraints in Table 1 are respected. The null space accesses infinite solutions near \mathbf{I}_0 such that the optics requirements are unchanged:

$$\mathbf{B} \Delta \mathbf{I}_C = \mathbf{B} \Delta \mathbf{I}_0 \quad (4)$$

This optimization method also has the advantage of applying other constraints to mitigate beam losses. The beta function at collimators near IR8 were made sure to be below the original value to reduce risk of beam loss and collimator damage shown in Table 1. However, there is no guarantee that a solution can be found for a given optics movement depending on the initial lattice and the constraints employed, and one may have to relax the constraints or move to a nonlinear method with a well-defined inverse.

Each movement of s_x^* produces the resulting current values, optics, and magnet strengths. The current values are inspected to confirm no current limits were violated; all other values were inspected to confirm optimization, correctness, and accuracy.

We have demonstrated that solutions can be found in range of ± 0.5 meters for the proton-proton lattice and are sufficient for our purpose of sPHENIX collision point optimization. The resulting magnet strengths are then stored in trim files for each movement of s_x^* and sent to machine during experiment.

3. Optics Measurement Methods

The TBT data is generated after the beam is kicked by a corrector (ARTUS) around IR6. The data shown in Fig. 3 upstream of IR6 yields centroid positions for 1024 turns in 168 and 167 horizontal and vertical BPMs respectively. A horizontal corrector first kicks the beam in the horizontal plane, then a vertical kick is applied after 500 turns to minimize coupling [11].

The TBT data is first centered to emphasize deviations from the original trajectory, allowing clearer observation of beam responses. This is most clearly pronounced near the IRs. The data is also truncated to 200 turns to remove transverse coupling effects present in later turns. The horizontal and vertical planes were treated separately while following the same analysis procedure. Since AC dipoles have been removed from RHIC tunnel, the data in this study has been analyzed with decoherence from nonlinear effects from nonlinear effects as well as chromatic detuning in mind [14].

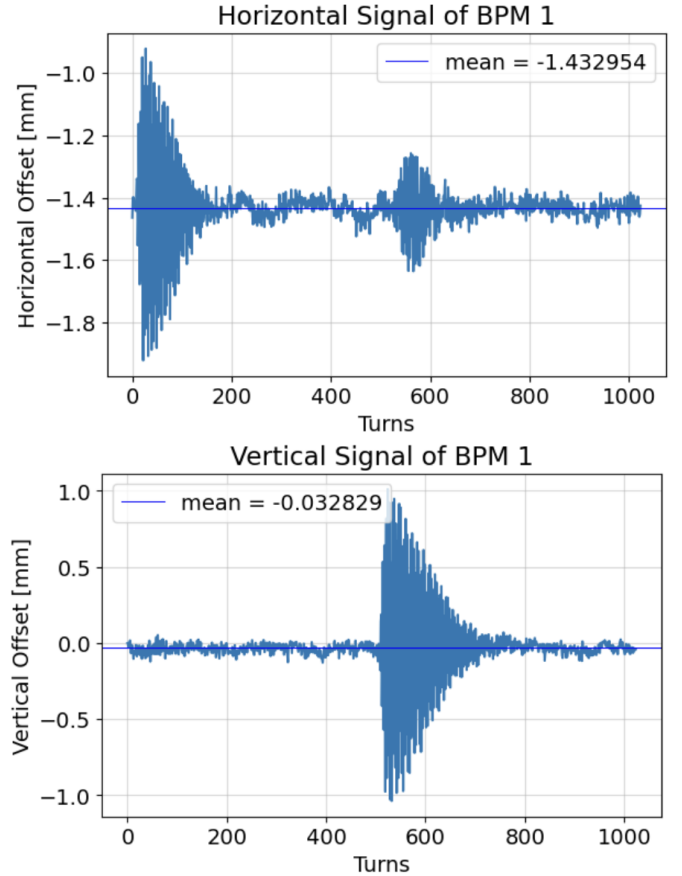


Figure 3: TBT data from BPM upstream of IP6 for 1024 turns. The top plot shows the horizontal axis and the bottom plot shows the vertical axis.

Table 1: Optics constraints used to optimize the magnet solutions.

Constraint	Definition	Notes
PS Limits	$I_j^{\min} + 5A \leq I_j \leq I_j^{\max} - 5A$	$j \in N_{\text{magnets}}$
Change in Current Strengths	$\max(\Delta I_j) \leq 5A$	$j \in N_{\text{magnets}}$
Hysteresis	$\ K_j^i\ \leq \ K_j^{i+1}\ $	$i \in N_{\text{iterations}}, j \in N_{\text{magnets}}$
Collimator at IR8	$\beta_u^i \leq \beta_u^0$	$i \in N_{\text{iterations}}, u \in \{x, y\}$

BPMs exhibiting tune deviations significantly different from the nominal machine working point are classified as unreliable or "bad" BPMs. To preserve the integrity of the dataset, such BPMs are excluded from the analysis by zeroing their signals. A tune offset outside of ± 0.005 was used as a criterion for exclusion.

3.1. One Turn Map

3.1.1. Ordinary Least Squares (OLS)

The one-turn map can be constructed using BPM data at IRs since they are drift space regions. Within such regions the angle coordinate can be analytically computed. RHIC currently has twelve operating drift space regions that can be used to calculate the one turn map: four IRs, and one drift space downstream and upstream of each IR in the blue ring. For this paper, we focus on the analysis at IR8, as presented in Section 4 since SPHENIX is located at IR8, although all other IRs follow similar analysis procedures. The detector solenoid is turned off at IR8. Within each drift region, the angle coordinate u'_{12} can be calculated between the two endpoints u_1 and u_2 of the drift space (downstream and upstream bpms) through Eq. (5):

$$u'_{12} = \frac{u_2 - u_1}{L} \quad (5)$$

Where L is the length of the drift space taken from [3]. u represents the horizontal or vertical axis. The equation for the one turn map is of the form:

$$\mathbf{Y} = \mathbf{M}_j \mathbf{X} \quad (6)$$

where:

$$\mathbf{X} = \begin{bmatrix} u \\ u' \end{bmatrix}^i \quad (7a)$$

$$\mathbf{Y} = \begin{bmatrix} u \\ u' \end{bmatrix}^{i+1}_j \quad (7b)$$

contains position and angle coordinate information of the dataset for the i^{th} and $(i+1)^{\text{th}}$ turn and the j^{th} bpm respectively, and

$$\mathbf{M}_j = \begin{bmatrix} \cos \phi + \alpha \sin \phi & \beta \sin \phi \\ -\gamma \sin \phi & \cos \phi - \alpha \sin \phi \end{bmatrix} \quad (8)$$

is the one turn map at the j^{th} bpm [22].

Eq. (6) represents a standard linear regression problem. This can be solved using an ordinary least squares algorithm (OLS), shown in Eq. (9) [5]:

$$\mathbf{M}_j = (\mathbf{X}^T \mathbf{X})^{-1} \mathbf{X}^T \mathbf{Y} \quad (9)$$

This was used to calculate the components of \mathbf{M}_j at each drift space. The linear optics (ϕ, α, β) at the j^{th} BPM can then be computed using the elements of \mathbf{M}_j :

$$\phi = \cos^{-1}\left(\frac{M_j^{11} + M_j^{22}}{2}\right) \quad (10a)$$

$$\beta = \frac{M_j^{12}}{\sin \phi} \quad (10b)$$

$$\alpha = \frac{M_j^{11} - M_j^{22}}{2 \sin \phi} \quad (10c)$$

Using OLS on RHIC BPM data is analogous to moment calculations of the BPM data used in [17, 22]. Since the equations from both methods are derived from the One Turn Map, both methods produce equivalent results. An additional 4D parameterization was also implemented to the one turn map to address concerns regarding coupling effects [6]; however, no significant coupling effects were observed in RHIC TBT data.

OLS depends on certain assumptions, which include linearity and homoscedasticity between \mathbf{X} and \mathbf{Y} , independence of errors, a lack of co-linearity between dependent variables, and errors-in-variables [5]. Homoscedasticity assumes the variance between variables in \mathbf{Y} remains constant for all values of the independent variables \mathbf{X} . This assumption is satisfied since BPM errors do not increase with respect to time, thus the variance between the current and next turn also remains stable. Linearity between \mathbf{X} and \mathbf{Y} is also respected since they are related via drift space, nonlinear effects are negligible compared to BPM errors, and decoherence from RHIC BPM data occurs slowly enough to justify a linear approximation over small timescales (200 turns). BPM errors arise from various, uncorrelated sources such as BPM gains, rolls, and magnet imperfections [16], therefore independence of errors is also respected.

The co-linearity between dependent variables is not violated from Eq. (5). The angle coordinate is constructed using both upstream and downstream BPMs, while OLS relies on the angle coordinate and only one of those BPMs. Therefore, the potential impact from co-linearity onto dependent variables is mitigated in this context.

The errors-in-variables assumption states that the independent variables \mathbf{X} contain no errors. However, BPM data is used in both \mathbf{X} and \mathbf{Y} for OLS and violates this assumption. As a

consequence, as the error in X increases, the estimated $\hat{\mathbf{M}}_j$ becomes increasingly biased downward, leading to an underestimation of the measurement \mathbf{M}_j . This is known as attenuation bias as shown in Eq. (11):

$$\hat{\mathbf{M}}_j = \mathbf{M}_j \frac{\sigma_x^2}{\sigma_x^2 + \sigma_\delta^2} \quad (11)$$

where σ_x is the intended range of values that the BPM data can take, and σ_δ is BPM error [5]. One solution to address this is to use a total least squares (TLS) calculation.

3.1.2. Total Least Squares (TLS)

Unlike OLS, TLS attempts to minimize the error in both X and Y , namely \mathbf{E} and \mathbf{F} . Eq. (6) then becomes:

$$\text{argmin}_{\mathbf{M}_j, \mathbf{E}, \mathbf{F}} \|\begin{bmatrix} \mathbf{E} & \mathbf{F} \end{bmatrix}\|_F \quad (12a)$$

$$\mathbf{Y} + \mathbf{E} = \mathbf{M}_j(\mathbf{X} + \mathbf{F}) \quad (12b)$$

Where $\|\cdot\|_F$ denotes the Frobenius norm. A derivation assuming a unique solution is described in detail in [8]. The idea is that a singular value decomposition (SVD) of the concatenation of \mathbf{X} and \mathbf{Y} is taken:

$$[\mathbf{X} \quad \mathbf{Y}] = [\mathbf{U}_X \quad \mathbf{U}_Y] \begin{bmatrix} \Sigma_x & 0 \\ 0 & \Sigma_Y \end{bmatrix} [\mathbf{V}_{XX} \quad \mathbf{V}_{XY}]^* \quad (13)$$

and the solution for \mathbf{M}_j is given by:

$$\mathbf{M}_j = -\mathbf{V}_{XY} \mathbf{V}_{YY}^{-1} \quad (14)$$

The algorithm aims to reduce the noise in both X and Y by selecting high variance, orthogonal modes that contribute to the one turn map while discarding low variance modes corresponding to BPM errors. All of the OLS assumptions still hold, with the additional requirement that a unique solution exists. Since a unique one-turn map exists between the two bpms at IR, this condition is satisfied.

3.2. Curve Fit

The calculation of a least-squares fitting method on BPM data will be referred to as the curve-fitting method (CF) throughout this paper, and is standard beta from amplitude method. Since the BPM data at RHIC exhibits decoherence, the fitting model must account for this effect in order to accurately represent the measured beam dynamics. The decoherence model from [14] is simplified to minimize the amount of parameters used for a nonlinear least-squares fit while maintaining the structure of closed-orbit oscillations, given by Eq. (15), where only the decoherence due to chromatic effects are included. A BPM signal over n turns is modeled with an amplitude a , a decoherence coefficient b , the machine tune ν , and the phase offset ϕ .

$$x_{co} = a \exp\left(\frac{-2\pi n^2}{b^2}\right) \cos(2\pi \nu n + \phi) \quad (15)$$

This least-squares fit is applied to all BPMs excluding the unreliable BPMs. The amplitudes of each BPM are then collected

into a vector \mathbf{A} and the beta function depends on the square of the amplitudes. A ratio (similar to the action [7]) is then calculated from the amplitudes and model beta function from arc sections and multiplied to the square of the amplitudes from Eq. (16) to get the measured beta values (β^{meas}) over the whole ring:

$$\beta^{meas} = (A)^2 \frac{\langle \beta_{arc}^{mod} \rangle}{\langle A_{arc} \rangle} \quad (16)$$

The arc section values were chosen due to the smaller values of the beta function in those regions generally yielding less errors than those in the IRs [16].

3.3. Linear Optics at IP

The linear optics parameters β^* and s^* at the IP were extracted using the β -function measured at BPMs located at the IRs. This was done using a nonlinear least squares fit to the following standard form of the β -function near a waist [22]:

$$\beta_{IR}(s) = \beta^* + \frac{(s - s^*)^2}{\beta^*} \quad (17)$$

Since transverse s^* values are not directly reported in MAD-X Twiss output files, model values of s^* were also calculated with this method using Eq. (17) with model β at IRs as inputs. The model values of β^* and s^* were then to be compared to experimental measurements to assess the accuracy of the optics measurement methods and the consistency with the lattice model.

3.4. Error Analysis

An error analysis study was done to measure the difference between OLS and TLS as well as to measure the robustness of the optics measurement methods presented. A beam tracking simulation using Xsuite was done using the RHIC lattice [9]. Two proton beams were simulated to match the amplitude and decoherence of RHIC BPM data for 200 turns. These were then tracked for 168 horizontal and 167 vertical BPMs. BPM errors are gaussian and propagated through Monte Carlo simulations. The error analysis procedure was equivalent in both planes, and results for only the horizontal plane is presented in this section.

3.4.1. OLS vs TLS

When comparing OLS vs TLS, TLS is expected to improve the β measurement at all IPs from OLS since there is noise in both X and Y due to BPM errors. What we find is partially true, shown in Fig. 4. Although only two BPMs are shown, g5-bx represent the BPMs at high-beta IRs (g5-bx, g6-bx, g7-bx, g8-bx) and g9-bx at low-beta IRs (g9-bx, g10-bx, g11-bx, g12-bx). Each group has similar graphs; BPMs at high-beta regions have better β measurements using TLS and BPMs at low-beta regions using OLS. We also see that TLS tends to overestimate while OLS tends to underestimate. Although both methods don't do well under very high noise, one is closer to the model than the other at a reasonable amount of noise in each group.

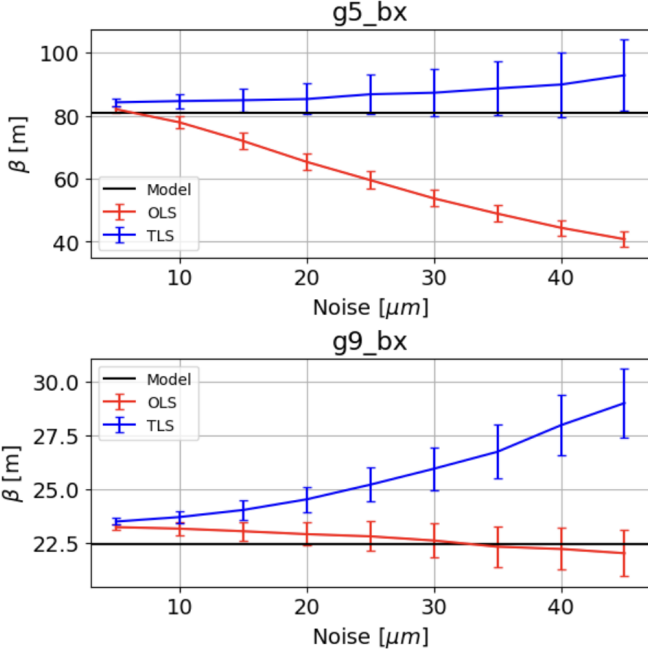


Figure 4: Simulated beta measurements from OLS (red) and TLS (blue) vs BPM error level from 5 to $50\mu\text{m}$. The solid black lines indicate model beta at BPM g5-bx (top) and BPM g9-bx (bottom). Error bars were calculated using a Monte Carlo simulation of 500 iterations for each noise level.

To understand why there is a discrepancy between TLS and OLS at high and low beta regions, a separate simulation was done to continuously transition from a high to low beta region. The BPM data was simulated using Eq. (15) instead of Xsuite. At each IR, RHIC BPM estimations of the fit parameters a, b, ν, ϕ were given. Varying each of these except for the machine tune, the phase offset is then mostly responsible for β at a BPM, and is what determines a high and low beta IR.

Holding a, b, ν constant, the phase at one BPM is held constant and the phase at the other BPM was varied from $[-2\pi, 2\pi]$. For IP6, the phase at BPM g5-bx was varied as shown in Fig. 5. By doing this, we can visualize scenarios where IP6 has a different beta squeeze by varying ϕ . A gaussian noise of $30\mu\text{m}$ was given to the simulated TBT data, and OLS and TLS was performed for each ϕ . Fig. 5 reflects the results from Fig. 4 where TLS follows the model curve more closely while OLS underestimates the measurement. The model curve represents β measurements using OLS without noise.

Similar measurements were made for the other IRs. For IP10, the phase at BPM g9-bx was varied as shown in Fig. 6. The figure resembles Fig. 5 (and any other IR); however, the OLS method fits the model closer than TLS. From this, we can more clearly see that OLS does better in low-beta regions and TLS in high-beta regions.

If the amplitudes of the BPM data is increased for the low-beta regions while keeping the BPM noise level constant, Fig. 6 will change to resemble Fig. 5. This then shows that OLS and TLS measurements will improve with higher signal to noise ratios (SNR).

TLS does worse than OLS at low beta due to the low SNR.

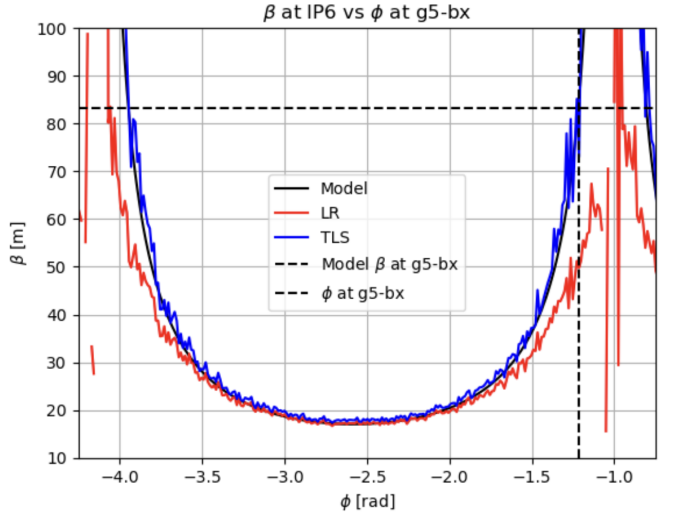


Figure 5: Simulated beta measurements from OLS (red) and TLS (blue) vs phase at g5-bx, zoomed in at $\phi = [-4.5, -5]$. The solid black line indicate model beta at BPM g5-bx. The dashed black lines indicate the model β and the model phase at the g5-bx BPM

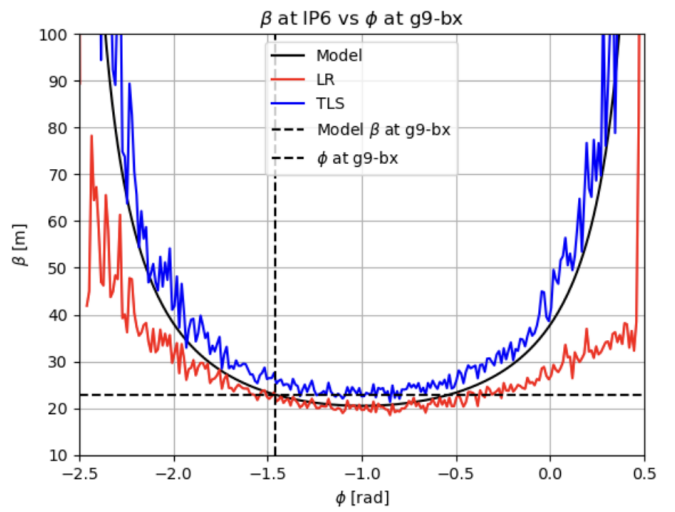


Figure 6: Simulated beta measurements from OLS (red) and TLS (blue) vs phase at g9-bx, zoomed in at $\phi = [-2.5, .5]$. The solid black line indicate model beta at BPM g9-bx. The dashed black lines indicate the model β and the model phase at the g9-bx BPM

OLS, while it underestimates the result, will always be conservative and stable. Stability can be measured using the condition number of $X^T X$ from Eq. (9) since the inverse of this expression determines the stability of OLS [5]. A relatively high condition number was measured in high-beta regions ($\approx 10^4$) and a low condition number in low-beta regions ($\approx 10^2$), showing relatively higher stability in low-beta regions. OLS is also conservative since although the SNR is low, the algorithm only consider noise in Y . TLS, on the other hand, considers and attempts to correct the noise in both X and Y . Since the noise overwhelms the signal, the algorithm's SVD step will tend to over-correct for the noise.

One can consider increasing the amplitudes of the BPM data when measuring β using TLS at low-beta. However, this will also increase the amount of noise in the signal. Therefore, when using the one-turn map to calculate β , TLS should be used for high-beta regions while OLS will be used for low-beta regions. For this paper, TLS will be used to present the results for IP8, a high-beta region.

3.4.2. Errors of Optics Measurement Methods

A rewritten version of the CF method and a harmonic analysis (HA) method from [2] using a Fourier decomposition of BPM data were used to compare to the measurement results of the one-turn map methods (OLS and TLS). The same particle tracking was used, and errors are once again added to the BPM signals. These errors are propagated into the β measurement, and the resulting β measurement errors propagate into the calculation of β^* and s^* . This was all done using 50 Monte Carlo iterations for each noise level.

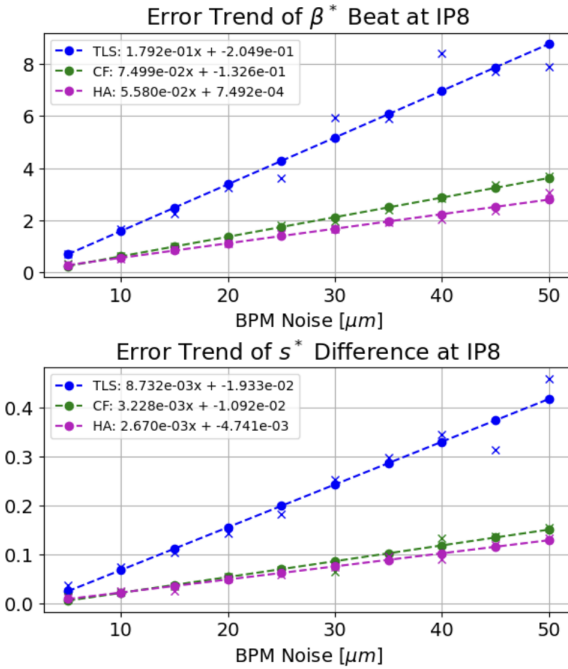


Figure 7: Error trends of TLS (blue), CF (green), and HA (magenta) vs BPM error level from 5 to $50\mu\text{m}$ for β^* beat (top) and s^* difference (bottom). The x's represent the standard deviation values used for the linear regression calculation of the error trends at IP8.

The standard deviations from the Monte Carlo method for the calculation of β^* and s^* are given by Fig. 7. The trend of these standard deviations are expected to be linear, and a linear regression was used to calculate the error trends. Although TLS improves the OLS measurement at IP8, the figure shows that errors from CF and HA are lower. This is primarily due to the overestimation of β measurements in TLS.

The corresponding error of β beat and s^* difference calculations from each optics measurement method can then be calculated using the error trends in Fig. 7. The resulting respective errors were used when analyzing experimental data using each optics measurement method in Section 4.

4. Experimental Results

The beam for this study consists of 12 proton bunches in the blue ring at RHIC. After the beams were in store, initial TBT measurements were taken. Since the insertion quadrupoles at IP8 have been unaltered, the data taken corresponds to $\Delta s_x^* = 0$.

The magnet strengths were then moved to $\Delta s_x^* = .1\text{m}$ according to the trim file produced by B corresponding to the appropriate Δs_x^* . After the movement, two TBT measurements were taken. The beam loss rate, tune, and beta around collimators are then monitored after every Δs_x^* movement to ensure no significant beam loss. The magnet strengths are also monitored to ensure correctness and to confirm that magnet strengths have been altered. This procedure was repeated afterward for $\Delta s_x^* = .3, .5\text{m}$ and again for backwards movement: $\Delta s_x^* = -.1, -.3, -.5\text{m}$.

After the TBT data had been gathered, the linear optics around IRs were then measured through the RHIC optics program (R-OP) as well as TLS, CF, and HA. Upon observing the Δs^* measurements at IP8, all methods demonstrate on average the correct general trend of appropriate s^* movement. This can be seen in Fig. 8 for Δs^* in both planes; the majority of measurements of all methods are all positioned near 0. This validates the methods mentioned in Section 2. However, each method show distinct results in terms of beta beat and s^* difference.

At each Δs^* movement, a comparison between all of the optics measurement methods are made for β^* and s^* around the IRs. Fig. 8 specifically shows the calculations for β^* beat and s^* difference in both planes at IP8, measured by the optics measurement methods with error bars calculated from Section 3.4.2. These errors are propagated from a BPM noise level of $30\mu\text{m}$. The noise from the TBT data was measured to be similar to that found in [16], where non-arc BPMs have slightly more error on average than arc BPMs at RHIC. The error bars for R-OP are calculated from Fig. 2. From the figure, TLS, CF, and HA all measure a smaller β^* beat and s^* difference than R-OP. Furthermore, their measurements are also overall more consistent around 0 (taken to be the model), and with one another, shown by the error bars. This shows that TLS, CF, and HA are also make more consistent measurements than R-OP.

This is further quantitatively shown in Table 2, where the average values are calculated from Fig. 8. TLS, CF, and HA clearly show more accurate and consistent values of star measurements than R-OP. However, the error values of TLS closely

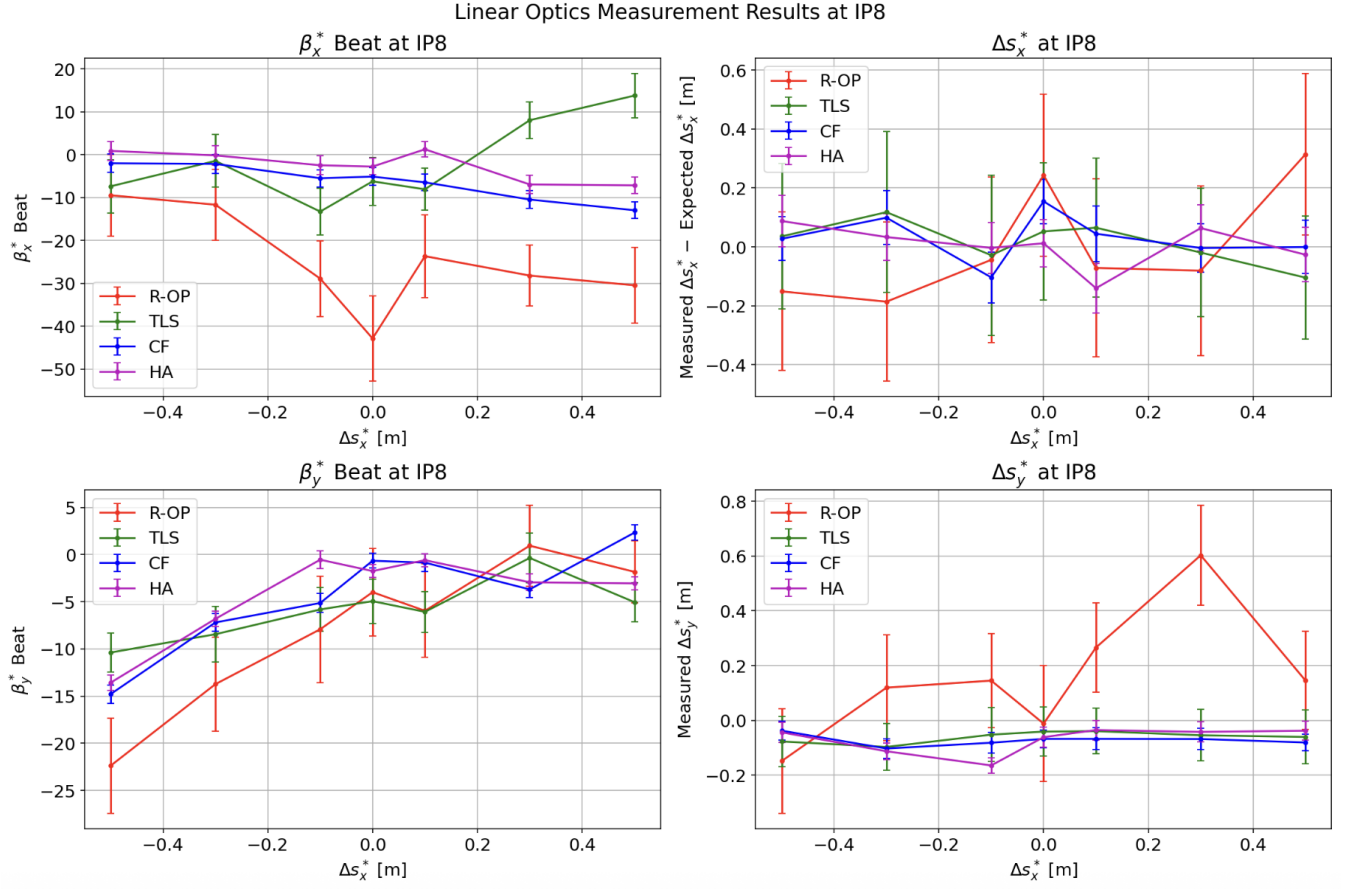


Figure 8: The average between two measurements for each Δs_x^* movement were taken and plotted. Measurements of β^* beat and s^* difference at IP8 were calculated using R-OP, TLS, CF, and HA. The expected value of Δs_x^* (s_x^* difference) was subtracted out of the measured values to match the structure of the other graphs. A BPM error level of $30 \mu\text{m}$ was chosen for IP8.

Table 2: β^* beat and s^* difference averaged over s_x^* movements for each optics measurement method.

Method	β_x^* Beat	s_x^* Difference [m]	β_y^* Beat	s_y^* Difference [m]
R-OP	25.030 ± 7.962	0.155 ± 0.272	0.810 ± 4.774	0.205 ± 0.181
TLS	8.460 ± 5.378	0.060 ± 0.243	5.866 ± 2.460	0.063 ± 0.094
CF	6.415 ± 2.138	0.061 ± 0.089	5.086 ± 0.906	0.072 ± 0.036
HA	3.730 ± 1.963	0.052 ± 0.078	4.652 ± 0.783	0.071 ± 0.031

matches that of R-OP for s_x^* , suggesting that TLS does not always improve the accuracy of s_x^* in this case.

When comparing TLS with CF and HA, CF and HA seem to agree more with the model than TLS. This is expected since CF and HA are model-dependent methods, and bias may be introduced when calculating the action, which depends on model and machine optics. On the other hand, TLS presents results that decrease the β^* beat and s^* difference from R-OP, producing results closer to but not as close to the model as CF and HA. Since measuring absolute accuracy of the optics is not possible, TLS, CF, and HA all present possible values for IP8 since they are consistent with each other.

Given this evaluation method, s_x^* and s_y^* differences show consistent measurements around the model and each measurement method besides R-OP. s_y^* difference is shown to be around $\sim 1\text{m}$, and s_x^* difference has more variation between s_x^* movement but still measures around 0. The β_x^* beat measurements show a slight negative drift between s_x^* movement. A similar case in β_y^* beat where even R-OP shows that as s_x^* is moved in the negative direction, the β_y^* beat increases substantially. This shows that improvements can be made in optics control, as non-linear magnetic effects could induce disparity between machine and model. Nevertheless, \mathbf{B} , while not perfectly, is able move the optics such that there is not too much measurement variation between s_x^* movements.

The errors obtained in s_y^* difference from TLS, CF, and HA show that error within $\pm 10\text{ cm}$ is possible for collisions at sPHENIX vertex. However, the same cannot be confidently said with s_x^* when using TLS. While it is likely the case that accurate measurement methods will need to be used such as CF and HA, TLS should still yield accurate results on average, comparable with CF and HA. For average β^* beat in IP8, TLS is shown to predict 10% within 5–6% accuracy, and CF and HA is shown to predict < 7% within 2% accuracy in x and within 1% in y. This shows an accurate beta beat measurement between methods and confirms the stability of beta at IP8 when moving s_x^* .

5. Conclusion

The sensitivity matrix \mathbf{B} was shown to consistently move the magnets such that s_x^* can be changed appropriately while not perturbing the other optics as well as obeying certain machine constraints. This was shown with all the linear optics methods, as the measurements of s_x^* moved appropriately while the other optics throughout the ring remained relatively unchanged. This method to move s_x^* can be extended to moving s^* in both transverse directions while taking care of the similar constraints as before.

TLS was shown to improve measurement of linear optics from OLS at high-beta regions such as IP6 and IP8. This is due to X and Y having built-in errors from BPMs. At high-beta regions, the SNR is still high enough where TLS will separate the noise from the system and produce meaningful measurements. However, OLS should still be used at low-beta regions such as IP10 and IP12 if there is a consistent noise between BPMs.

TLS, CF, and HA were then able to measure a lower average β^* beat and s^* difference at IP8 than R-OP when moving s_x^* . The difference in results between TLS and CF/HA is explained by higher error bars and model-dependent vs model independent methods. Using these methods lowers the β^* beat down to less than 10% with a consistency of 1–2%. However, CF and HA shows the consistency of s_x^* is around $\pm 10\text{ cm}$, while TLS measures $\pm 24\text{ cm}$. Future studies to lower this estimate down within TLS method should be examined to be comparable with the model-dependent methods.

The difference between R-OP and the other optics measurement methods could be due to unintentional errors in the calculation. Therefore, the methods used to calculate the linear optics at RHIC will be updated in the future as well as for additional measurement methods to be included. Other methods to measure linear optics at IP can also be analyzed and compared to such as MIA methods with PCA/ICA as well as N-BPM methods. Additional model-dependent methods to analyze and compare to the TLS method may also strengthen the quality of these types of measurements.

This study is a preliminary one used to build confidence in s^* movement. In future experiments, Bayesian Optimization (BO) will be used to locate the optimal luminosity collision region within sPHENIX. Improving accuracy of s^* movement will improve the accuracy of the s^* request from BO to RHIC. Other experiments may also apply these techniques to improve the accuracy and consistency of the movement of linear optics for other kinds of experiments.

Acknowledgements

This work is supported by DOE Office of Nuclear Physics under award number DE-SC0023518. This work is also supported by Brookhaven Science Associates, LLC under Contract No. DE-SC0012704 and DE-AC02-06CH11357 with the U.S. Department of Energy.

References

- [1] Campbell, S., 2017. sphenix: The next generation heavy ion detector at rhic. *Journal of Physics: Conference Series* .
- [2] Castro, P., 1996. Luminosity and Beta Function Measurement at the Electron-Positron Collider Ring LEP. Ph.d. thesis. CERN.
- [3] Collider-Accelerator-Department, 2006. RHIC Configuration Manual. Technical Report. Brookhaven National Laboratory.
- [4] Deniau, L., Grote, H., Roy, G., Schmidt, F., 2024. The MAD-X Program (Methodical Accelerator Design), Version 5.08.01: User's Reference Manual. European Organization for Nuclear Research (CERN). URL: <https://mad.web.cern.ch/madx/>. editor: Laurent Deniau.

[5] Draper, N.R., Smith, H., 2014. Applied regression analysis. Wiley.

[6] Edwards, D.A., Teng, L.C., 1973. Parametrization of linear coupled motion in periodic systems. *IEEE Transactions on Nuclear Science* 20, 885–888. doi:10.1109/tns.1973.4327279.

[7] Fischer, W., 2003. Robust linear coupling correction with n -turn maps. *Phys. Rev. ST Accel. Beams* 6, 062801. doi:10.1103/PhysRevSTAB.6.062801.

[8] Golub, G.H., van Loan, C.F., 1980. An analysis of the total least squares problem. *SIAM Journal on Numerical Analysis* 17, 883–893. doi:10.1137/0717073.

[9] Iadarola, G., Maria, R.D., Łopaciuk, S., Abramov, A., Buffat, X., Demetriadou, D., Deniau, L., Hermes, P., Kicsiny, P., Kruyt, P., Latina, A., Mether, L., Paraschou, K., Sterbini, G., Veken, F.F.V.D., Belanger, P., Niedermayer, P., Croce, D.D., Pieloni, T., Riesen-Haupt, L.V., Seidel, M., 2024. Xsuite: An integrated beam physics simulation framework. *JACoW HB2023* , TUA211.

[10] Langner, A., Benedetti, G., Carlà, M., Iriso, U., Martí, Z., Coello de Portugal, J., Tomás, R., 2016. Utilizing the n beam position monitor method for turn-by-turn optics measurements. *Phys. Rev. Accel. Beams* 19, 092803. doi:10.1103/PhysRevAccelBeams.19.092803. (Received 20 March 2016; published 21 September 2016).

[11] Liu, C., 2014. Optics Measurement and Correction During Beam Acceleration in the Relativistic Heavy Ion Collider. Technical Report. Brookhaven National Laboratory (BNL). Upton, NY, United States.

[12] Liu, C., Kewisch, J., Huang, H., Minty, M., 2019. Minimization of spin tune spread for preservation of spin polarization at rhic. *Phys. Rev. Accel. Beams* 22, 061002.

[13] de Maria, R., Schmidt, F., Skowronski, P.K., 2006. Advances in matching with MAD-X, in: Proceedings of the International Computational Accelerator Physics Conference (ICAP), Chamonix, France. pp. 213–215. CAP06-TUPLT041.

[14] Meller, R.E., 1987. Decoherence of Kicked Beams. Technical Report. Fermilab.

[15] Minty, M.G., Zimmermann, F., 2003. Transverse optics measurement and correction: Multiknobs, optics tuning, and monitoring, in: Measurement and Control of Charged Particle Beams. Springer Nature, pp. 43–46.

[16] Shen, X., Lee, S.Y., Bai, M., White, S., Robert-Demolaize, G., Luo, Y., Marusic, A., Tomás, R., 2013. Application of independent component analysis to ac dipole based optics measurement and correction at the relativistic heavy ion collider. *Phys. Rev. Accel. Beams* 16, 111001. doi:10.1103/PhysRevSTAB.16.111001.

[17] Syphers, M.J., Miyamoto, R., 2007. Direct measurements of beta-star in the tevatron. *IEEE Transactions on Nuclear Science* .

[18] Tomás, R., Aiba, M., Franchi, A., Iriso, U., 2017. Review of linear optics measurement and correction for charged particle accelerators. *Physical Review Accelerators and Beams* 20. doi:10.1103/physrevaccelbeams.20.054801.

[19] Wang, C., Sajaev, V., Yao, C., 2003. Phase advance and β -function measurements using model-independent analysis. *Phys. Rev. Accel. Beams* 6, 104001. doi:10.1103/PhysRevSTAB.6.104001.

[20] Wegscheider, A., Langner, A., Tomás, R., Franchi, A., 2017. Analytical n -beam position monitor method. *Phys. Rev. Accel. Beams* 20, 111002. doi:10.1103/PhysRevAccelBeams.20.111002.

[21] Werner, H., Muratori, B., 2006. Concept of luminosity, in: CERN Accelerator School: Intermediate Course on Accelerator Physics, CERN, Zeuthen, Germany. pp. 361–378. CERN-2006-002.

[22] Wiedemann, H., 2015. Particle Accelerator Physics. Fourth ed., Springer Nature.